Original Research Article: full paper

(2022), «EUREKA: Physics and Engineering»
Number 4

QUALITY COMPARISON OF Y-SHAPE JOINTS BY TUBE HYDROFORMING WITH AND WITHOUT COUNTERFORCE

Quang Vu Duc
Department of Machines & Fundamentals of Machine Design[1]

Duy Dinh Van✉
Department of Metal Forming[2]
Duy.dinhvan@hust.edu.vn

Trung Nguyen Dac
Department of Metal Forming[2]

Quang Nguyen Huu
Department of Mechatronics[1]

[1]*University of Economics – Technology for Industries*
456 Minh Khai, Vinh Tuy Ward, Hai Ba Trung District, Hanoi, Vietnam, 100000

[2]*Hanoi University of Science and Technology*
1 Dai Co Viet, Bach Khoa ward, Hai Ba Trung district, Hanoi, Vietnam, 100000

✉**Corresponding author**

Abstract

The design capability, strength, and structural rigidity provided by tube hydroforming (THF) are successfully used in many applications to produce high-strength parts and assemblies with improved mechanical properties, optimized service life, and weight features. In tubular metal forming, output parameters such as branch height, distribution of tube wall material thickness, distribution of damage factor, metal flow, effective stress, and effective strain significantly affect the quality of the product after the forming process. Therefore, this paper aims to evaluate the manufacturing quality of Y-shape joints from AISI304 material steel tube through output parameters of THF process with and without counter punch force on numerical simulation base. The Finite Element Method (FEM) has become an established feature of metal forming technology. The objective of FEM is to replace costly and elaborate experimental testing with fast, low-cost computer simulation. The simulation study uses finite element method-based virtual prototyping techniques to characterize output parameters, gain insight into strain mechanics, and predict mechanical properties of shaped components. The research results are presented clearly and unambiguously through the evaluation of 7 criteria to compare the quality of the specimens hydroformed by two surveyed cases and optimize the crucial input process parameters. And these data can be applied in experiments, more efficient product and process design, calculation, and control of input parameters avoiding costly trial and error in industrial production. The findings can help technologists optimize process parameters in the hydroforming process of products with protrusion from a tubular blank.

Keywords: tube hydroforming, Y-shaped joint, tubular metal forming, counter punch force.

DOI: 10.21303/2461-4262.2022.002256

1. Introduction

Reducing costs, reducing time, and improving products have always been the main goals of advanced metal forming processes. Therefore, much research on metal forming processes has been invested in and promoted over the years. In tube fabrication, tubular blanks show many advantages over tubes coiled from sheet blanks. These workpieces show lower plastic deformation and higher formability for subsequent forming operations [1, 2]. THF can be applied to various industrial fields, such as transportation, aerospace, and metal microtube fabrication [2, 3], based on the quality and different shapes of semi-finished and finished products.

Indeed, THF is a metal shaping method that plastically deforms a tube or two interlocked tubes according to the shape of the mold cavity through internal fluid pressure. Furthermore, axial punch feed and counterpunch can facilitate metal flow, leading to better plastic strain distribution during the shaping process (**Fig. 1**) [4].

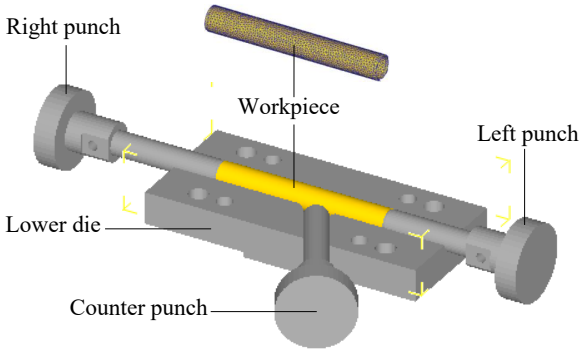

Fig. 1. The geometric model of the mold and the Y-shaped tube is designed in Solidworks software, and the workpiece is meshed

The THF process has many significant advantages, including reduced weight, reduced production time, lower tool cost, low spring back, and improved strength and rigidity of the structure [5, 6]. However, it presents some disadvantages, including expensive equipment, a lack of knowledge based on tool design and manufacturing processes, sealing problems, and poor thickness distribution [5, 6]. As for the main failure models, they are found to be bursting, wrinkling, and buckling. These failures are mainly related to the key input process parameters, tooling, and workpiece material [7, 8]. Among these factors, it is possible to refer more specifically to the load path [9], die design [10], friction at tube-tool interfaces [11], and material properties [6, 8]. The final thickness distribution in the deformed tube is strongly dependent on the tube material properties [12, 13] and is also extremely sensitive to the die radius, which can change the plastic strain flow in the radius region [13, 14].

The interaction between the tool and the components in the specific pipe hydrostatic stamping has three friction zones: the guide zone, the transition zone, and the extension zone [4]. Different lubrication regimes are required due to differences in local stress states and material strain states in the three friction regions [15]. Therefore, choosing a lubricant that works for all three friction zones will challenge the forming process. Studies have shown that by both experimental and FEA, different lubricants produce different friction and directly impact the quality of the deformed tube [14, 16, 17]. During each metal forming stage, the material structure is work-hardened to a certain degree, which gradually reduces the possibility of tubular forming [1]. The formability zone based on the limits, including leakage, yield start, wrinkling, fracture, and bursting, depends mainly on the correlation of axial punch force and internal fluid pressure [18]. Among them, local wrinkle is a common defect that often occurs during the forming process of thin-walled structures with a relatively wide range of axial punch force and internal fluid pressure. Therefore, they need to be effectively coordinated to avoid this wrinkling phenomenon. The prediction of wrinkling and fracture through FEM is mainly made by geometric, energy, and plastic dichotomy theory [19, 20]. The analysis of literary sources does not sufficiently cover the previously unresolved problem.

In this study, the team of authors used the finite element numerical simulation method by Deform 3D software version 6.1 [21] to compare the effective heights and thickness distribution of tube wall material in the two cases of shaping with and without counterpunch. And also analyze the distribution of damage factors, material flow, effective stress, effective strain, and load-stroke in the specimens. Thereby evaluating the quality of Y-shaped joints from AISI304 by the THF process. From the research results of these two simulation cases, the team has come to some conclusions for the next step to conduct a physical experiment in order to compare with the results obtained in the future.

2. Materials and Methods

2. 1. Hydroforming part and original workpiece

THF is a complicated metal shaping process that involves structural geometrical dimensions, workpiece material properties, and various process parameters. In this study, AISI304 steel was selected as the tube material used in numerical simulation. The material properties are unaltered and summarized in Table 1; the tubular blank and Y-shape tube with the geometrical parameters are shown in **Table 2**.

Table 1

Material parameters and properties of AISI304 steel

Material parameters and properties	Value [22, 23]
Temperature (°C)	24
Density, ρ (kg/m^3)	7850
Young's modulus, *E* (GPa)	193
Hardening coefficient, *K* (MPa)	1471
Work hardening exponent, *n*	0.584
Prestrain, ε_0	0.06
Poisson's ratio, *n*	0.3
Yield strength (MPa)	230
Ultimate tensile strength (MPa)	480
Elongation (%)	40
Hardness (HB)	183 max

Table 2

Tubular blank and Y-shape tube

Parameters	Symbol/unit	Value
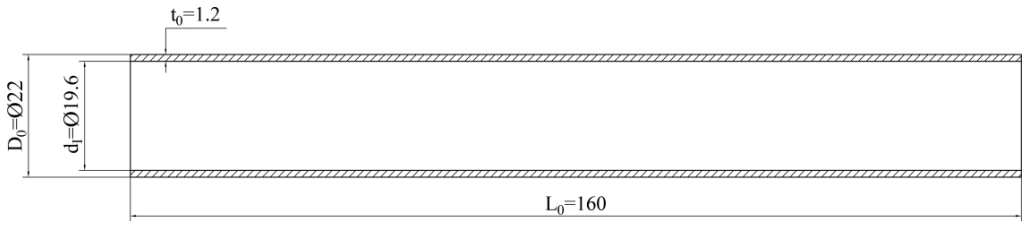		
Outside diameter of tube	D_0 (mm)	22
Inside diameter of tube	d_I (mm)	19.6
Initial thickness of tube	t_0 (mm)	1.2
Initial length of tubular blank	L_0 (mm)	160
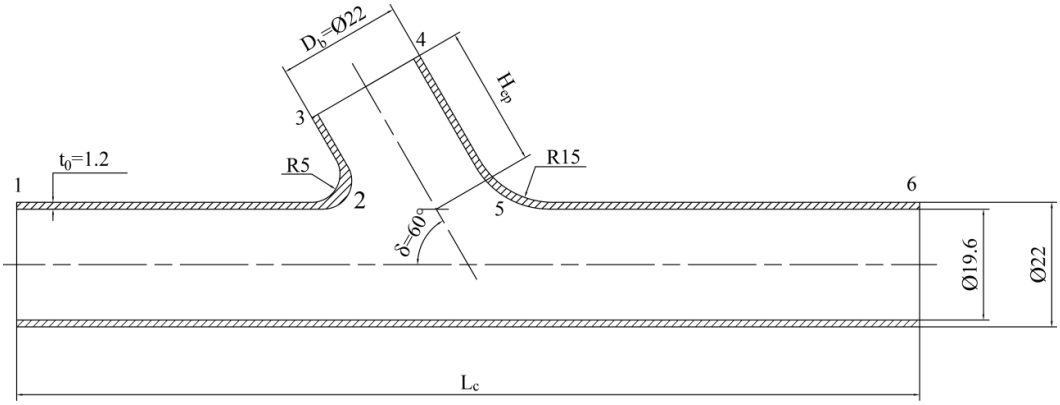		
Branch angle	δ(^{0})	60
Total height of the branch	H_{tb} (mm)	to be designed
Efficient height of the branch	H_{eb} (mm)	to be designed
Diameter of branch	D_b (mm)	22
Leftward fillet radius	R_{lf} (mm)	5
Rightward fillet radius	R_{rf} (mm)	15
Component length	L_c (mm)	to be designed

2. 2. Numerical simulation

Finite element analysis and finite element method have enabled the construction of almost all practical metal forming processes, including complex 3-D forming operations. As a result, the researcher can now clearly visualize the THF process and study the plastic flow behavior, stress, residual stress, back spring, destruction, and other shaping conditions inside fabricated parts [4, 24, 25]. High efficiency and low-cost finite element industrial numerical simulation are used in this study to analyze and compare the quality of hydroformed Y-tubes with and without counter punch. The geometry, dimensions, and materials of the mold and workpiece are modeled to be consistent with the actual manufacturing of the product (**Fig. 1**).

In the geometric model setting for the simulation, the models were built in five parts: flexible tube blank, rigid lower die half, rigid upper die half, rigid left punch and rigid right punch (**Fig. 1**). Only the plastic deformation behavior of the workpiece is studied and meshed with 3D tetrahedral elements in the present analysis. To ensure the accuracy and convergence of the FE simulation, the tubular blank was set as a plastic deformation type and meshed by 45,000–50,000 tetrahedral elements with an absolute mesh pattern.

For each type of hydroformed product, important input parameters such as internal fluid pressure P_i, axial punch feed (axial punch displacement velocity), and lubrication conditions (coefficient of friction) are determined. Refer to document [4] for these input parameters. Numerical simulations were carried out with the process parameters having the following values: internal fluid pressure $P_i = 40$ MPa, 70 MPa, 100 MPa, and 130 MPa; right axial punch displacement velocity $v_{right} = 1$ mm/s ($l_{right} = 25$ mm), left axial punch displacement velocity $v_{left} = 2v_{right} = 2$ mm/s ($l_{left} = 2l_{right} = 50$ mm), total stroke 75 mm; shear friction coefficient $\mu = 0.05$ (the mixed layer lubrication) [26–28].

3. Results and discussion

From the numerical simulation results of the two case studies above, the research team compared the output parameters of the part to be shaped. These include effective height, distribution of material wall thickness, damage factor, effective strain, effective stress, material flow, and load in the load-stroke curve in the specimens.

3. 1. Effective height of the branch

When the pressure P_i increases by 30 MPa, the effective height of branch H_{eb} increases correspondingly by an average of about 2.48 mm with the counter punch, while when the effective height of branch decreases at $P_i = 130$ MPa without the counter punch (H_{eb} (130 MPa) = 17.3 mm < $< H_{eb}$ (100 MPa) = 20.99 mm) because the material thinning ratio (above measurement position 3) is $\gamma_i = 100\ \%\cdot(t_i - t_0)/t_0 = 100\ \%\cdot(0.74 - 1.2)/1.2 = -38.33\ \%$ (**Fig. 2**), which is greater than the maximum allowable thinning ratio of – 25 % [29]. From **Table 3**, it is possible to see that at low internal pressure without counter punch for higher effective height. Meanwhile, the higher internal liquid pressure with a counter punch gives a higher effective height than without a counter punch.

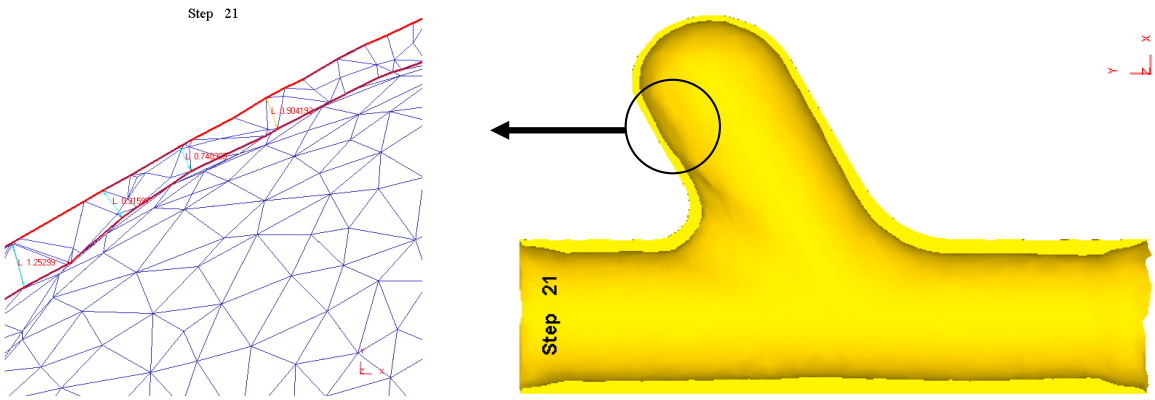

Fig. 2. The position of the product is thinned beyond the 25 % limit

Table 3

Effective height comparison with and without counterpunch in the specimens

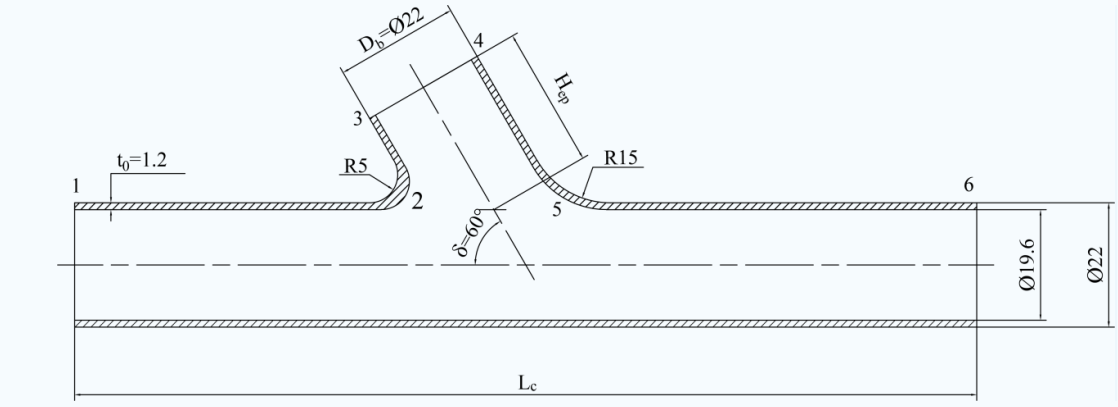

	H_{eb} without counterpunch (mm)		H_{eb} with the counterpunch (mm)	
40	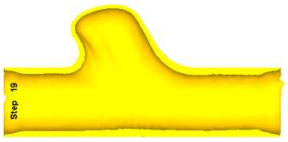	15.1	11.85	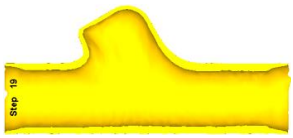
70	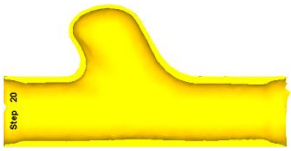	16.53	15.45	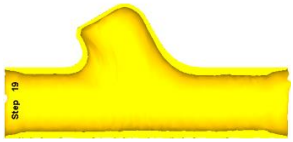
100	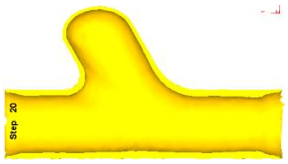	20.99	17.12	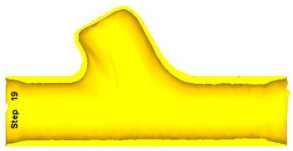
130	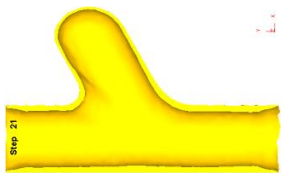	17.3	19.29	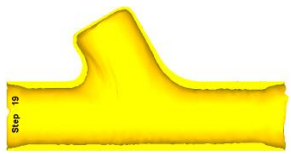

Subsequent comparisons of THF with and without counterpunch will be analyzed with internal fluid pressure $P_i = 130$ MPa, $v_{right} = 2v_{left} = 2$ mm/s, total stroke 75 mm; Shear coefficient of friction $\mu = 0.05$.

3. 2. The distribution of tube wall material thickness

With the initial workpiece thickness $t_0 = 1.2$ mm, **Fig. 3** shows a similarity in the strong trend of increasing material thickness from measured point 1 ($t_{i1} = 1.77$ mm, thickening ratio $\gamma_{i1} = 100\,\% \cdot (t_{i1} - t_0)/t_0 = 47.5\,\%$, $t_{i1} = 2.1$ mm, $\gamma_{i1} = 75\,\%$) to measured point 2 ($t_{i2} = 1.88$ mm, $\gamma_{i1} = 56.67\,\%$, $t_{i2} = 2.13$ mm, $\gamma_{i1} = 77.5\,\%$), they were distributed in the left end of the tube in both cases. At the right end of the tube, the point is measured 6 ($t_{i6} = 2.19$ mm, $\gamma_{i6} = 82.5\,\%$, $t_{i6} = 2.44$ mm, $\gamma_{i6} = 103.33\,\%$) and 5 ($t_{i5} = 2.1$ mm, $\gamma_{i5} = 75\,\%$, $t_{i5} = 2.55$ mm, $\gamma_{i5} = 112.5\,\%$) has a stronger increase in material thickness compared to the left end of the tube in both cases. However, with the counter punch, let's obtain a larger thickness than without the counter punch at these measuring points.

At the top of the branch formed without counter punch, the thickness of the measured point 3 was slightly increased ($t_{i3} = 1.25$ mm, $\gamma_{i3} = 4.17\,\%$), of the measured point 4 slightly de-

creased (t_{i4} = 1.12 mm, γ_{i4} = –6.67 %). With a counter punch, measured points 3 and 4 have reduced thickness t_{i3} = 1.11 mm, γ_{i3} = –7.5 % and t_{i4} = 1.01 mm, γ_{i4} = –15.83 %, respectively, due to material flow velocity is limited.

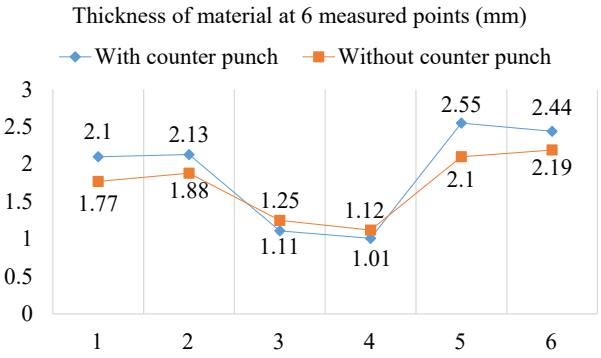

Fig. 3. Comparison of material wall thickness distribution in specimens

3. 3. The distribution of damage factor in the specimen

Fig. 4 show the distribution of damage factor concentrated mainly in the shaped branch; the *H* region without counterpunch has a value of 1.06 more significant than 1; this value indicates a high fracture probability.

In the case of simulation with a counter punch, the distribution of the damaging factor has the largest value of 0.891 also in the *H* region, showing that no fracture has occurred. It proves that the part is formed successfully without any errors.

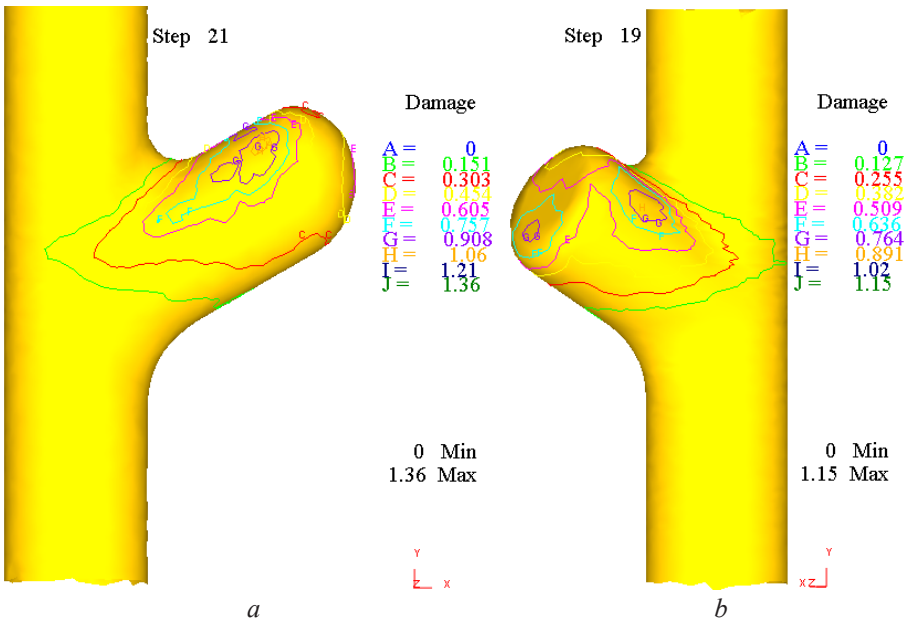

a *b*

Fig. 4. Comparison of the damage factor distribution in the specimens:
a – without counter punch; *b* – with counter punch

3. 4. The distribution of effective stress in the specimens

As shown in **Fig. 5**, the effective stress distribution has similar characteristics for the two ends of the tube and branch with and without counter punch.

However, the stress distribution on the product with a counter punch is larger and more uniform, concentrated at 977 MPa (max 1090 MPa) compared to 936 MPa (max 1040 MPa) without a counter punch.

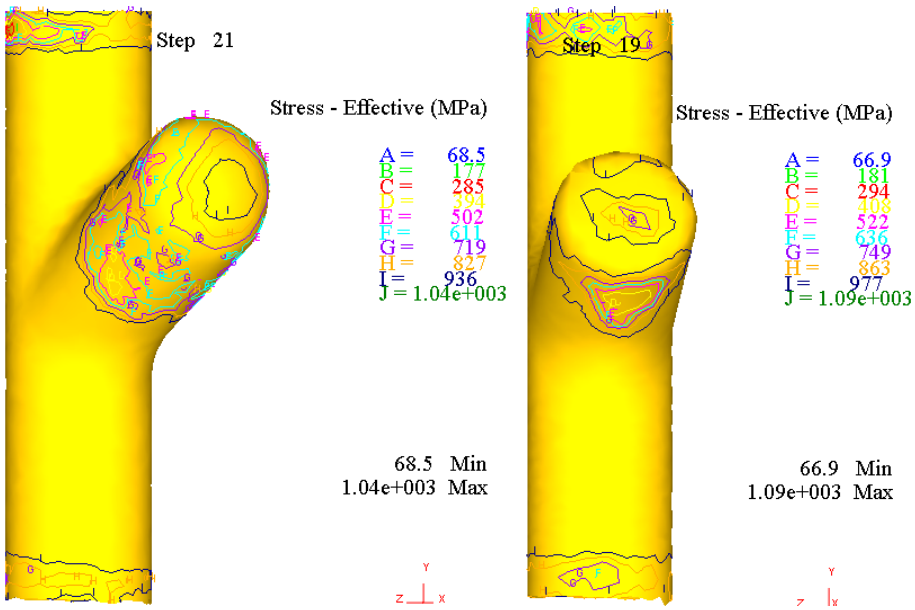

a *b*

Fig. 5. Comparison of the effective stress distribution in the specimens:
a – without counter punch; *b* – with counter punch

3. 5. The distribution of effective strain in the specimens

Observing the effective strain distribution in the samples of the two cases, as shown in **Fig. 6**, it can be seen that the workpiece is deformed in all three zones during the forming process. The expansion zone has the strongest deformation; without a counter punch, the value is concentrated in the range of 0.733 mm/mm to 2.04 mm/mm; with a counter punch, the concentration value is in the field of 0.493 mm/mm to 1.34 mm/mm. These values represent more favorable plastic deformation in the mold cavity with a counter punch because, according to the law of minimum strain resistance, the metal flow will preferentially flow through the position with a smaller resistance.

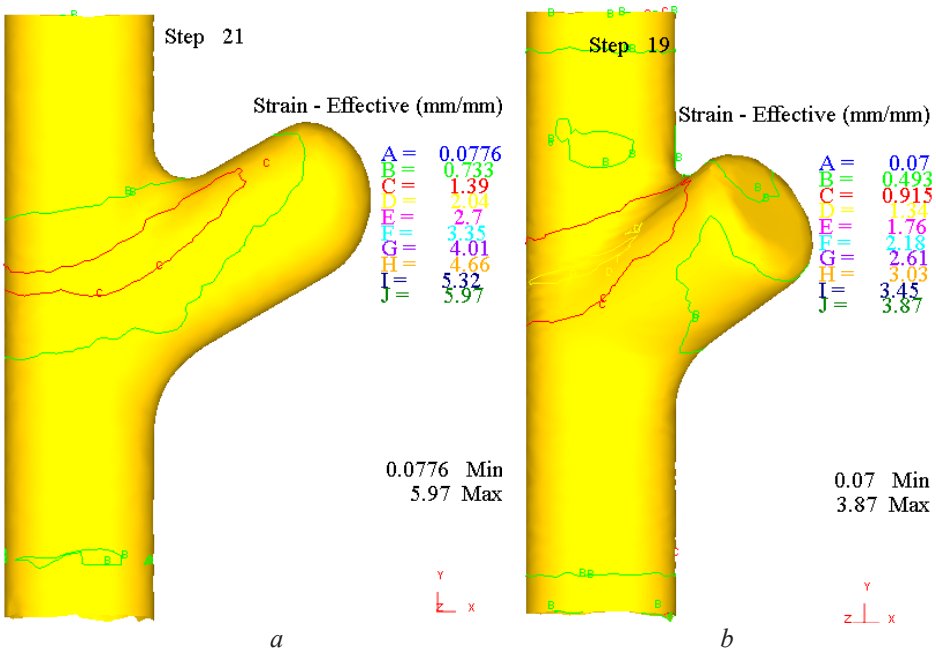

a *b*

Fig. 6. Comparison of the effective strain distribution in the specimens:
a – without counter punch; *b* – with counter punch

In the case of forming with a counter punch, the effective strain distribution has the largest value of 3.87 mm/mm compared with 5.97 mm/mm without a counter punch, which shows the advantage of plasticized flow with a counter punch.

3. 6. The distribution of material flow velocity in the specimens

The distribution of material flow velocities in both cases (**Fig. 7**) has its maximum value at the right end of the tube at 2 mm/sec.

In both cases, the material flow velocity at the left end of the tube is also equivalent to 0.9 mm/sec. However, there is a significant difference; the material flow velocity without a counter punch reaches a value of 1.35 mm/sec, two times larger than the flow velocity with a counter punch. Those results in a greater total branch height and the thinning ratio at the top without counterpunch ($H_{tb\ without} = 34.98$ mm, $\gamma_{itb\ without} = -38.33$ %) and with the counter punch ($H_{tb\ with} = 22.18$ mm, $\gamma_{itb\ with} = -37.5$ %).

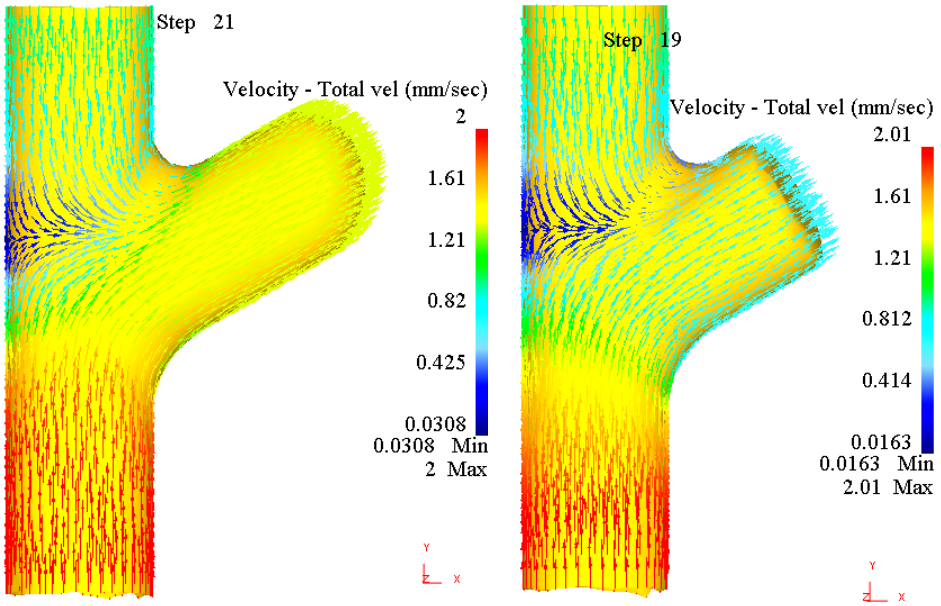

a *b*

Fig. 7. Comparison of the material flow velocity distribution in the specimens: *a* – without counter punch; *b* – with counter punch

3. 7. The distribution of load on the load-stroke curve in the specimens

From the load-stroke graph of the two cases, as shown in **Fig. 8**, in the absence of counter punch at 25 mm axial punch stroke, the left and right axial punch loads are $P_{left\ axial\ (without\ counter\ punch)} = 18.6T$ and $P_{right\ axial\ (without\ counter\ punch)} = 14.7T$ (**Fig. 8, *a***), respectively. In the case of using a counter punch with the power limit graph as shown in **Fig. 9, *a***, the axial punch load has a larger value than the case without a counter punch, including $P_{left\ axial\ (with\ counter\ punch)} = 21.9T$, $P_{right\ axial\ (with\ counter\ punch)} = 16.6T$ (**Fig. 8, *b***), and $P_{counter\ punch} = (P^2_{X\ Load} + P^2_{Y\ Load})^{1/2} = (3.91^2 + 2.56^2)^{1/2} = 4.67T$ (**Fig. 9, *b, c***). The load value of the left axial punch during the forming process in both cases with and without counter punch is larger than the load value of the right axial punch because the axial feed stroke of the left punch is two times the axial feed stroke of the right punch ($l_{left} = 2l_{right} = 50$ mm). In the case of using a counter punch with the load value of counter punch $P_{counter\ punch} = 4.67T$, the left axial punch force and right axial punch force has a larger value, respectively $21.9–18.6 = 3.3T$ and $16.6–14.7 = 1.9T$ compared with the case of without counter punch because the expansion zone of the protrusion is affected by the counter punch force, which reduces material flow velocity into the mold cavity during the forming process (**Fig. 7**). This leads to the need for a higher axial load value to meet the sealing requirements and to feed the material into the expansion zone as designed.

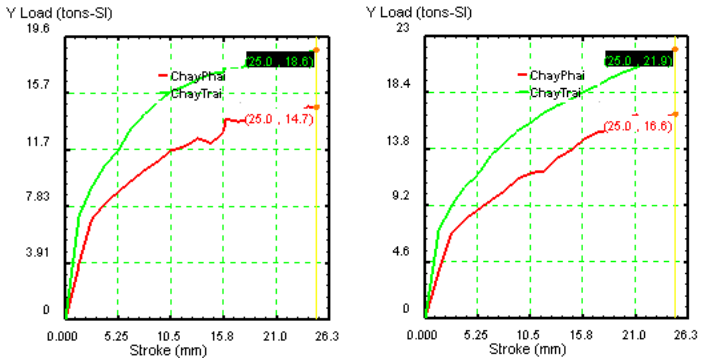

a *b*

Fig. 8. Comparison of load distribution on the load-travel curve in the specimens (–ChayPhai = –Right axial punch, –ChayTrai = –Left axial punch): *a* – without counter punch; *b* – with a counter punch

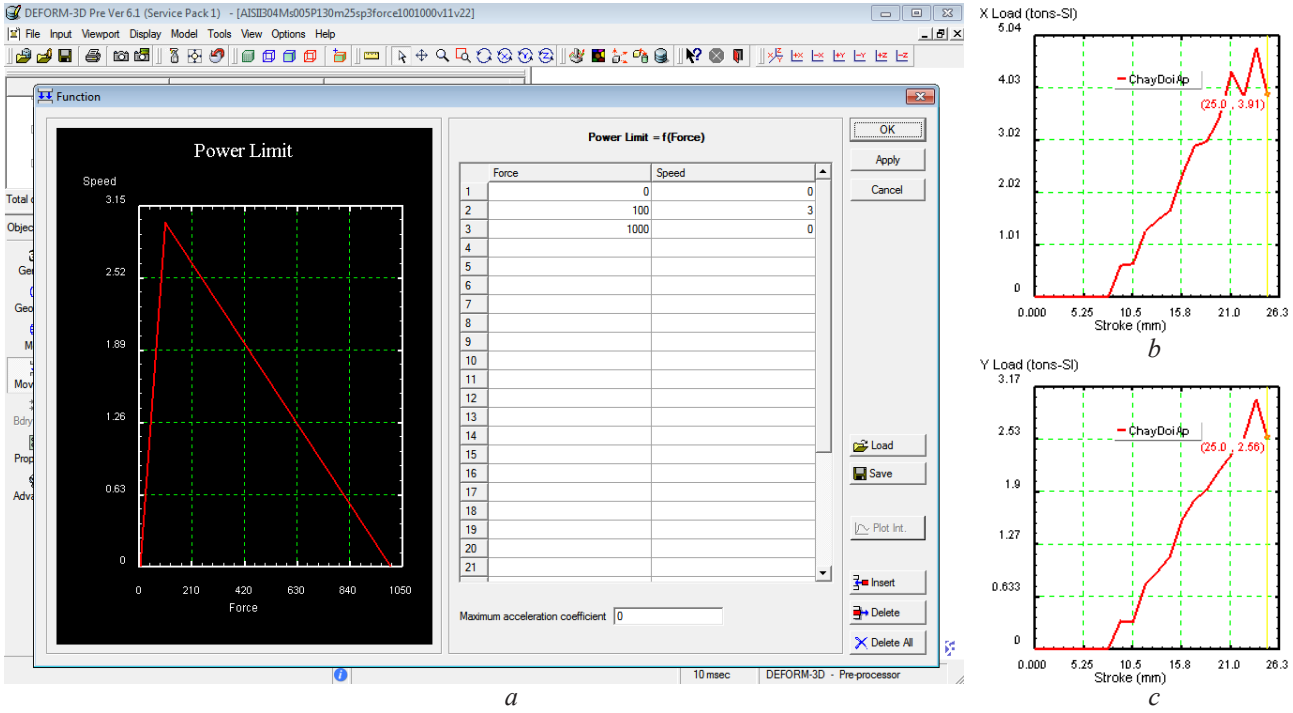

a *b* *c*

Fig. 9. Power limit graph and load-stroke graphs along the OX and OY axes of the counter punch (–ChayDoiAp = –Counterpunch): *a* – Power limit graph used in Deform 3-D; *b* – Load-stroke graphs along the OX axes of the counter punch; *c* – Load-stroke graphs along the OY axes of the counter punch

The load-stroke curves of both axial punches were stable throughout the process, indicating the suitability and success of the THF process. On the load-stroke graphs, an unsTable value segment appears at the end of the stroke, proving that the branch's total height has reached the limit value.

The limitations of this study that should be noted are the ideal control assumptions by numerical simulation of load paths and lubrication procedures compared with the actual conditions of their implementation. Realistic control of load paths, including internal pressure, axial feed and counter force, is a challenge, especially for the counter force when increasing in value will lead to a very large thinning rate of the tubular wall material and/or perforation in the top of protrusion. The condition of mixed layer lubrication with shear coefficient $\mu = 0.05$ is assumed to be the same in three different types of friction zone, namely, guiding zone, transition zone, and expansion zone. The lubrication methods are different because of the difference in the local state stress mode and

substance deformation mode that is in the friction areas. Therefore, choosing a lubricant that is active in all friction zones is also challenging.

The fabrication of high-quality products using THF faces many challenges, such as inappropriate combinations of internal pressure, axial feed, and/or counter punch, thereby resulting in necking, wrinkling or tearing in different sections of formed products. Components with high structural strength have been constantly in demand in the industry. The Y-shaped tubes selected for the study are used in oil and gas industries and pipe fitting systems. The development of this study makes a new contribution by comparing seven criteria to evaluate the quality of the specimens hydroformed by two investigated cases, thereby optimizing the crucial input process parameters for each case of the THF process.

4. Conclusions

This paper analyzed seven criteria, including Effective height of the branch, The distribution of tube wall material thickness, The distribution of damage factor in the specimens, The distribution of effective stress in the specimens, The distribution of effective strain in the specimens, The distribution of material flow velocity in the specimens and The distribution of load on the load-stroke curve in the specimens to compare the quality of hydrogen-formed Y-tubes with and without counter punch. The results of the finite element simulation with the input parameters are shown in Section 2. 2, and the above analysis shows that both the formed cases have advantages and disadvantages.

In the absence of a counter punch, the quality of the branch is guaranteed when the internal liquid pressure is less than $P_i = 130$ MPa.

In the case of using a counter punch, the branch's quality is guaranteed at low and high internal fluid pressure, optimizing process parameters and plastic deformation in the mold cavity. However, the control of counterforce will make the THF process more complicated. In return, the damage factor distribution in the specimens is satisfactory; the effective stress distribution and effective strain are uniform; material flow velocities into the expansion zone are lower.

The input and output parameters through numerical simulation have been analyzed to be suiTable for the successful forming process of Y-joints. The results of this study can be applied to the fabrication of similar tube parts and help technicians have a better insight into the process and quality of the product being hydroformed.

Acknowledgments

The team of authors would like to express their gratitude for the help of the University of Economics and Technology for Industries (https://uneti.edu.vn/) and Hanoi University of Science and Technology (https://www.hust.edu.vn/) during the implementation of this study.

References

[1] Abbassi, F., Ahmad, F., Gulzar, S., Belhadj, T., Karrech, A., Choi, H. S. (2020). Design of T-shaped tube hydroforming using finite element and artificial neural network modeling. Journal of Mechanical Science and Technology, 34 (3), 1129–1138. doi: https://doi.org/10.1007/s12206-020-0214-4

[2] Metal Forming Handbook (1998). Springer, 568. doi: https://doi.org/10.1007/978-3-642-58857-0

[3] Yasui, H., Yoshihara, S., Mori, S., Tada, K., Manabe, K. (2020). Material Deformation Behavior in T-Shape Hydroforming of Metal Microtubes. Metals, 10 (2), 199. doi: 10.3390/met10020199

[4] Duc Quang, V., Van Duy, D., Dac Trung, N. (2021). On the Formation of Protrusion and Parameters in the Tube Hydroforming. Mechanisms and Machine Science, 521–530. doi: https://doi.org/10.1007/978-3-030-91892-7_49

[5] Bell, C., Corney, J., Zuelli, N., Savings, D. (2019). A state of the art review of hydroforming technology. International Journal of Material Forming, 13 (5), 789–828. doi: https://doi.org/10.1007/s12289-019-01507-1

[6] Singh, H. (2003). Fundamentals of hydroforming. Society of Manufacturing Engineers, 219.

[7] Koç, M., Altan, T. (2001). An overall review of the tube hydroforming (THF) technology. Journal of Materials Processing Technology, 108 (3), 384–393. doi: https://doi.org/10.1016/s0924-0136(00)00830-x

[8] Manabe, K., Amino, M. (2002). Effects of process parameters and material properties on deformation process in tube hydroforming. Journal of Materials Processing Technology, 123 (2), 285–291. doi: https://doi.org/10.1016/s0924-0136(02)00094-8

[9] Li, S., Xu, X., Zhang, W., Lin, Z. (2008). Study on the crushing and hydroforming processes of tubes in a trapezoid-sectional die. The International Journal of Advanced Manufacturing Technology, 43 (1-2), 67–77. doi: https://doi.org/10.1007/s00170-008-1702-3

[10] Abdelkefi, A., Malécot, P., Boudeau, N., Guermazi, N., Haddar, N. (2017). On the tube hydroforming process using rectangular, trapezoidal, and trapezoid-sectional dies: modeling and experiments. The International Journal of Advanced Manufacturing Technology, 93 (5-8), 1725–1735. doi: https://doi.org/10.1007/s00170-017-0621-6

[11] Vollertsen, F., Plancak, M. (2002). On possibilities for the determination of the coefficient of friction in hydroforming of tubes. Journal of Materials Processing Technology, 125-126, 412–420. doi: https://doi.org/10.1016/s0924-0136(02)00292-3

[12] Tolazzi, M. (2010). Hydroforming applications in automotive: a review. International Journal of Material Forming, 3 (S1), 307–310. doi: https://doi.org/10.1007/s12289-010-0768-2

[13] Ngaile, G., Yang, C., Kilonzo, O. (2011). Real-Time Friction Error Compensation in Tube Hydroforming Process Control. Journal of Manufacturing Science and Engineering, 133 (6). doi: https://doi.org/10.1115/1.4005430

[14] Ahmadi, H., Zohoor, M. (2016). Investigation of the effective parameters in tube hydroforming process by using experimental and finite element method for manufacturing of tee joint products. The International Journal of Advanced Manufacturing Technology, 93 (1-4), 393–405. doi: https://doi.org/10.1007/s00170-016-9690-1

[15] Pham, V. N. (2007). Hydrostatic forming technology. Hanoi: Bach Khoa Publishing House.

[16] Reddy, P. V., Reddy, B. V., Ramulu, P. J. (2019). An investigation on tube hydroforming process considering the effect of frictional coefficient and corner radius. Advances in Materials and Processing Technologies, 6 (1), 84–103. doi: https://doi.org/10.1080/2374068x.2019.1707437

[17] Ngaile, G., Gariety, M., Altan, T. (2006). Enhancing Tribological Conditions in Tube Hydroforming by Using Textured Tubes. Journal of Tribology, 128 (3), 674–676. doi: https://doi.org/10.1115/1.2197849

[18] Asnafi, N. (1999). Analytical modelling of tube hydroforming. Thin-Walled Structures, 34 (4), 295–330. doi: https://doi.org/10.1016/s0263-8231(99)00018-x

[19] Teng, B., Yuan, S., Chen, Z., Jin, X. (2012). Plastic damage of T-shape hydroforming. Transactions of Nonferrous Metals Society of China, 22, s294–s301. doi: https://doi.org/10.1016/s1003-6326(12)61722-1

[20] Liu, N., Yang, H., Li, H., Yan, S. (2016). Plastic wrinkling prediction in thin-walled part forming process: A review. Chinese Journal of Aeronautics, 29 (1), 1–14. doi: https://doi.org/10.1016/j.cja.2015.09.004

[21] DEFORM-3D Post Ver 6.1 (Service pack 1).

[22] Jirathearanat, S., Hartl, C., Altan, T. (2004). Hydroforming of Y-shapes-product and process design using FEA simulation and experiments. Journal of Materials Processing Technology, 146 (1), 124–129. doi: https://doi.org/10.1016/s0924-0136(03)00852-5

[23] Gale, W. F., Totemeier, T. C. (Eds.) (2004). Smithells Metals Reference Book. Butterworth-Heinemann.

[24] Pandey, A. K., Walunj, B. S., Date, P. P. (2018). Simulation based approach for light weighting of transmission components using tube hydroforming. Procedia Manufacturing, 15, 915–922. doi: https://doi.org/10.1016/j.promfg.2018.07.405

[25] Ktari, A., Abdelkefi, A., Guermazi, N., Malecot, P., Boudeau, N. (2021). Numerical investigation of plastic flow and residual stresses generated in hydroformed tubes. Proceedings of the Institution of Mechanical Engineers, Part L: Journal of Materials: Design and Applications, 235 (5), 1100–1111. doi: https://doi.org/10.1177/1464420721989746

[26] Koç, M. (Ed.) (2008). Hydroforming for advanced manufacturing. Woodhead Publishing. doi: https://doi.org/10.1533/9781845694418

[27] Schey, J. A. (1984). Tribology in Metalworking: Friction, Lubrication, and Wear. Journal of Applied Metalworking, 3 (2), 173–173. doi: https://doi.org/10.1007/bf02833697

[28] Nielsen, C. V., Martins, P. A. F. (2021). Metal forming: Formability, Simulation, and Tool Design. Academic Press. doi: https://doi.org/10.1016/C2020-0-02428-X

[29] Koç, M., Allen, T., Jiratheranat, S., Altan, T. (2000). The use of FEA and design of experiments to establish design guidelines for simple hydroformed parts. International Journal of Machine Tools and Manufacture, 40 (15), 2249–2266. doi: https://doi.org/10.1016/s0890-6955(00)00047-x

Received date 15.03.2022
Accepted date 08.07.2022
Published date 30.07.2022

How to cite: *Duc, Q. V., Van, D. D., Dac, T. N., Huu, Q. N. (2022). Quality comparison of Y-shape joints by tube hydroforming with and without counterforce. EUREKA: Physics and Engineering, 4, 46–56. https://doi.org/10.21303/2461-4262.2022.002256*